The charge of micro-particles in a low pressure spatial plasma afterglow

The charge of micro-particles in a low pressure spatial plasma afterglow

B. van Minderhout,[1, a)] T. Peijnenburg,[2] P. Blom,[2] J.M. Vogels,[2] G.M.W. Kroesen,[1] and J. Beckers[1]
[1)] *Department of Applied Physics, Eindhoven University of Technology, PO Box 513, 5600 MB Eindhoven, The Netherlands*
[2)] *VDL Enabling Technologies Group, PO Box 80038, 5600 JW Eindhoven, The Netherlands*

(Dated: May 14, 2019)

In this letter, we present charge measurements of micro-particles in the spatial afterglow (remote plasma) of an inductively coupled low pressure radiofrequency plasma. The particle afterglow charge of $(-30 \pm 7)\,\mathrm{e}$, being deducted from their acceleration in an externally applied electric field, is about three orders of magnitude lower compared to the typical charge expected in the bulk of such plasmas. This difference is explained by a relatively simplistic analytical model applying Orbital Motion Limited theory in the afterglow region. From an application perspective, our results enable further understanding and development of *in situ* plasma-based particle contamination control for ultra-clean low pressure environments.

Utilizing the physical interaction between plasma and small particles is a promising way forward to enable *in situ* particle contamination control, especially in ultra-clean low pressure systems used for instance in material processing and high-end semiconductor industries[1]. The potential of such a plasma-based solution stems from the ability of plasmas to both electrically charge immersed particles (typical in the size range 10 nm to 10 µm)[2] and control particle trajectories by the high electric fields self-induced by the plasma[3].

In such dusty or complex plasmas, *i.e.* plasmas containing nano- to micrometer sized particles, the plasma-induced particle surface charge is known to be one of the key parameters driving elementary processes such as momentum transfer between streaming ions and the particle (i.e. the ion drag force[2,4]), local Debye shielding[5], Coulomb interaction with other particles[6](i.e. the interaction in strongly-coupled complex plasmas) and plasma-particle synthesis[7].

Plasma-charging of particles larger than 50 nm in size in the quasi-neutral plasma bulk is relatively well understood[8–12] and can be described by Orbital Motion Limited (OML) theory balancing the fluxes of charged plasma species towards the particle surface[13]. However, charging mechanisms are far from understood for regions where the plasma is not actively powered, for instance in the temporal or spatial plasma afterglow where plasma species are depleted and enter the regime of free diffusion rather than governing ambipolar diffusion where quasi-neutrality is no longer obeyed.

From an application point of view, it is especially this plasma afterglow that is dominantly important for both cleaning and production processes. For instance, due to the highly-transient plasmas present in Extreme Ultra-violet (EUV) lithography tools[14–17], particle interaction with both temporal and spatial plasma afterglows becomes crucial to achieve the cleanliness standards of the future[18,19]. Along the same trend of reasoning, potential contamination control strategies depend heavily on understanding the basic charging mechanisms, where particles in a low pressure gas flow are plasma-charged and consecutively deflected and removed using externally applied electric fields. However, the few plasma particle charging studies that were performed in this region are limited to temporal plasma afterglows[20–27] which differs fundamentally regarding the distinct evolution of plasma parameters, such as electron temperature and plasma density, compared to a spatial afterglow situation. This directly impacts the particle charging.

To bridge this gap in knowledge and to enable the development of future contamination control strategies, we present measurements of the residual charge on particles in a gas flow in the mbar pressure range after these particles have traveled through an inductively coupled plasma. In order to explain the measured charge which is more than three orders lower than the particle charge expected in the quasi-neutral plasma bulk[13], a simplistic analytical model is presented. As will be shown, experiment and model fit within a factor of 6.

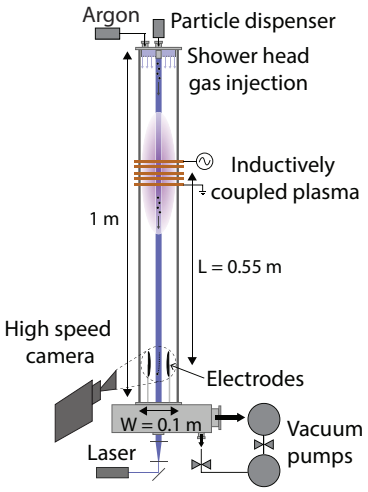

Figure 1. Schematic of the Plasma Particle Charging Investigation (PPCI) setup in which (from top to bottom) micro-particles fall through a spatially limited region of plasma after which their charge is measured by accelerating these particles in an externally applied electric field.

[a)] Electronic mail: b.v.minderhout@tue.nl

The experiments were carried out using the Plasma Particle Charging Investigation (PPCI) setup (Figure 1). In this setup, micro-particles were injected from the top and fell through a spatially limited region of plasma which charges the micro-particles electrically. Downstream of the active plasma regio, *i.e.* in the spatial plasma afterglow, the residual charge was measured by accelerating the particles in a direction perpendicular to this downstream velocity vector in an externally applied electric field. The main element of the PPCI setup was a square glass tube filled with argon at 0.9 mbar (the base pressure was 5×10^{-7} mbar). Monodisperse melamine formaldehyde (MF) particles were injected using a particle dispenser similar to those used in earlier studies[28,29]. These particles were (4.9 ± 0.2) µm in diameter and coated with a layer of silver of several hundred nanometers thickness to minimize triboelectric charging[30]. From the top of the tube, next to the particle injection, a 50 sccm argon flow was applied through a shower head helping the establishment of a laminar flow profile. This flow accelerated the particles to a measured settling velocity of $v_{p,f} = 0.36\,\mathrm{m\,s^{-1}}$ before particles and flow enter the active plasma region and ensured stable plasma conditions.

After injection, the particles passed through an inductively coupled plasma (ICP). The plasma discharge was generated by sending a radiofrequent (RF) current at 13.56 MHz through the coils. Inductively, about 15 W of power was coupled into the plasma. To verify that electron heating due to the remote electric RF fields from the ICP at the position of measurements were small, we estimated the maximum field strength to be $E_{RF} = 0.1\,\mathrm{V\,m^{-1}}$. This is indeed negligible with respect to the externally applied electric field of $E_{DC} = 4.3\,\mathrm{kV\,m^{-1}}$.

To study the particle trajectories the particles were illuminated by a vertical laser sheet of about 3 mm thickness and 40 mm width and imaged by a high speed camera (Photron Fastcam mini UX100) at 3200 fps. The plane of this laser sheet was perpendicular to the viewing direction of the camera. In order to study the charge of the plasma-charged particles, two Rogowski[31] shaped curved electrodes generated a DC electric field of $4.3\,\mathrm{kV\,m^{-1}}$, which accelerated the particles in the horizontal direction, *i.e.* perpendicular to the settling velocity vector and the viewing direction. The curved shape of these Rogowski electrodes suppressed the field enhancement near the edges of the electrodes. This resulted in an increased maximum electric field that could be applied without creating a DC glow discharge. The diameter of these electrodes was 70 mm with a separation distance of 40 mm, whereas the imaged area was 40×40 mm in the center of the electrodes. The electric field in this imaging region could be considered homogeneous by approximation.

Key in the charge measurement in this letter was the horizontal acceleration which the residual charged particles experienced from the externally applied electric field. Once the temporal evolution of the horizontal component

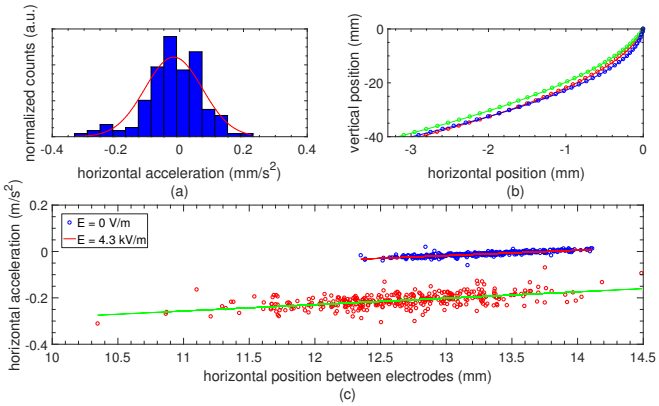

Figure 2. a) Histogram of the horizontal acceleration distribution for the situation without plasma, a stationary background gas and in the absence of an externally applied electric field. b)Three typical particle trajectories together with a quadratic fit in the region of externally applied electric field after passing the ICP. Every tenth data point is plotted for clarity, in addition the starting point of each trajectory is transformed to the origin. c) Plot of the measured horizontal acceleration as a function of the horizontal distance between the electrodes. Each blue circle depicts a particle that traveled through the plasma with a 50 sccm flow in the absence of the externally applied electric field, whereas each red circles depicts particle a particles that was subject to an electric field of $E = 4.3\,\mathrm{kV\,m^{-1}}$ and for the rest identical conditions as the blue circles. The origin of the x-axis is at the left electrode as seen from the position of the camera.

x of the particle trajectory was found, the horizontal acceleration $\mathrm{d}^2x/\mathrm{d}t^2$ could be retrieved. Realizing that this acceleration was caused by the electric field E working on the particle charge Q, Newton's second law could be used to find the charge of the particles with mass m as $Q = (m/E)\left(\mathrm{d}^2x/\mathrm{d}t^2\right)$. The power of this measurement technique is that the individual charge of multiple particles could be measured simultaneously as long as all particles were within the imaging region.

To verify that measurements errors such as lens aberrations and particle detection mistakes are extremely small, we have plotted the horizontal acceleration distribution from 148 trajectories which traveled through a stationary argon gas in the absence of plasma and externally applied electric field in Figure 2a. The mean $(3 \times 10^{-5}\,\mathrm{m\,s^{-2}})$ and standard deviation $(1 \times 10^{-4}\,\mathrm{m\,s^{-2}})$ of Figure 2a show that the measurements errors are indeed small. Furthermore, it can be concluded that the mutual Coulomb interaction between particles due to their triboelectric charge is negligible, *i.e.* particles do not repel or attract each other.

Figure 2b shows three typical particle trajectories falling in the region of externally applied electric field after they have passed the ICP together with a quadratic fit for each trajectory. These fits overlap clearly with the data points. From this it can be concluded that there is no significant neutral drag acting in horizontal direc-

tion on the micro-particles obscuring our measurements. Note that the neutral drag scales with horizontal particle speed $v_{p,x}$ and would therefore lower the net force on the particles as they are accelerated in the electric field.

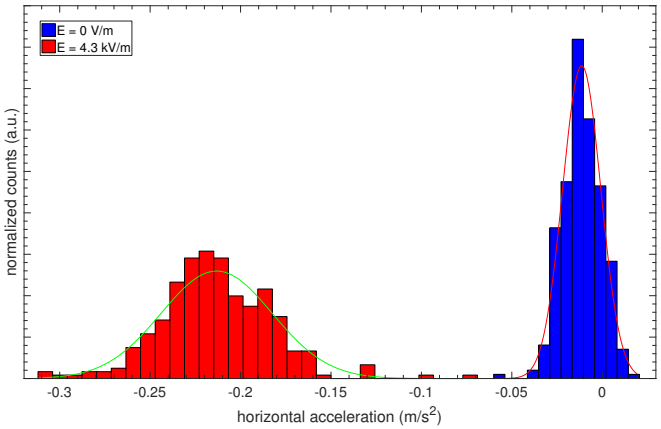

Figure 3. Particle charge measurement in the form of two acceleration distribution. The distribution in blue is composed of 319 particles that traveled through the plasma afterglow in the absence of externally applied electric field, whereas the distribution in red is composed of 297 particles that were subject to an electric field of $E = 4.3\,\mathrm{kV\,m^{-1}}$.

Figure 3 shows the particle charge measurement in the form of two horizontal acceleration distributions. The distribution in blue shows the horizontal acceleration of the particles after passing the plasma discharge with a 50 sccm flow in the absence of the externally applied electric field. The mean ($a_f = -1.2 \times 10^{-2}\,\mathrm{m\,s^{-2}}$) and standard deviation ($\sigma_f = 2.0 \times 10^{-2}\,\mathrm{m\,s^{-2}}$) are significantly larger than those in Figure 2a. We believe that flow disturbances around the electrodes cause the acceleration distribution to broaden with respect to the distribution in Figure 2a. The red distribution shows the measured acceleration, with a mean value of $a_p = -2.1 \times 10^{-1}\,\mathrm{m\,s^{-2}}$, for the situation where the electric field is switched on, while all other parameters are identical to the blue distribution. It is the clear shift between the two acceleration distributions in Figure 3 from which the particle charge is obtained $Q = (-30 \pm 7)\,\mathrm{e}$

The standard deviation of the red distribution in Figure 3 ($\sigma_p = 4.4 \times 10^{-2}\,\mathrm{m\,s^{-2}}$) is about a factor two larger than σ_f due to two reasons. Firstly, the particles have a spread in Q/m because variations in size lead to variations in charge[13] and mass, each scaling differently with size. Secondly, purely monodisperse particles also have a spread in charge due to the stochastic nature of the plasma charging currents arriving at the particle surface, especially important for these low values of the particle charge in the afterglow. For monodisperse particles, Khrapak *et al.*[32] have shown that the coefficient $\delta = \sigma_Q/\sqrt{|Q|} = (0.46{-}0.50)$ for $T_e = (1{-}20)\,T_i$ (with T_e and T_i the electron- and ion temperature). For our measurements, $\delta \approx 1.3$, which is significantly higher than this theoretical value which makes us believe that the dominant cause of this difference is the spread in mass of our particles.

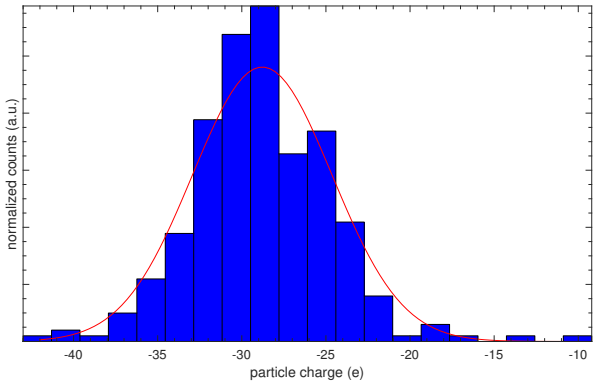

Figure 4. The measured particle charge distribution composed of 297 particles.

Figure 4 shows the measured particle charge distribution assuming σ_f to be zero. This charge distribution is obtained by subtracting a_f from a_p; the means of the blue and red distributions shown in Figure 3 and calculating the charge using Newton's second law using the supplier provided particle mass $m_p = 9 \times 10^{-14}\,\mathrm{kg}$.

The particle charge we have measured is about three orders of magnitude lower than the charge that would be expected in the plasma core[13] but is, however, still significant. To explain this charge we propose a simplistic analytical model describing the decharging of microparticles falling through an ICP, consecutively followed by its afterglow. Where in previous works such models have been used to analyse particle decharging in temporal plasma afterglows[20,21,24], our model extends the general thought and applies it to a spatial plasma afterglow. For now, we neglect the influence of ion-neutral collisions. The developed model consists of three typical timescales: the plasma-particle interaction timescale τ_{pp}, the particle charging timescale τ_Z and the electron temperature relaxation timescale τ_{T_e}. After introducing the timescales, the electron temperature T_e is estimated and finally the particle charge in the afterglow is obtained.

The plasma-particle interaction time τ_{pp} describes the typical time a particle resides within a plasma region with constant plasma-parameters and is defined by

$$\tau_{pp} = \frac{\lambda_D}{v_{p,f}} \equiv \frac{\tau_{pp}^0}{\sqrt{\tilde{n}}}. \tag{1}$$

Here, λ_D is the (linearized) Debye length, the smallest length scale on which plasma parameters can be considered constant, and $\tilde{n} = n_{e,i}/n_e^0$ the dimensionless plasma density, where n_e^0 is the initial plasma density at the position of the coils; here to be called the plasma core.

The particle charging timescale τ_Z represents the time needed for particles to reach their plasma-induced equi-

librium charge and is defined by[8]

$$\tau_Z = \frac{\lambda_{D_{i0}}^2}{v_{T_i} a} \frac{1}{(1+y)} \frac{1}{\tilde{n}} \equiv \frac{\tau_Z^0}{\tilde{n}}. \quad (2)$$

Here, $\lambda_{D_{i0}}$ is the initial ion Debye length, $v_{T_i} = \sqrt{8k_bT_i/\pi m_i}$ the thermal speed of the ions and $y = -eV(a)/k_bT_e$ the reduced particle potential with V the potential of the particle surface. Equation 2 originates from the Orbital Motion Limited (OML) theory[13] which evaluates the current balance of charged plasma species at the particle surface. Note that $\lambda_D > a$ everywhere in the afterglow, which justifies the use of OML theory[8].

The electron temperature relaxation timescale τ_{T_e} describes the typical energy loss time for the electrons in the afterglow region. Due to collisional energy losses, T_e relaxes which is described by $\mathrm{d}\tilde{T}_e \Big/ \mathrm{d}t = -(\tilde{T}_e - 1)/\tau_T$. The governed timescale for this relaxation is given by[33]

$$\tau_{T_e} = \sqrt{\frac{2}{\pi}} \sqrt{\frac{m_i}{m_e}} \frac{\lambda_{ea}}{v_{T_i}} \frac{1}{\sqrt{\tilde{T}_e}} \equiv \frac{\tau_{T_e}^\infty}{\sqrt{\tilde{T}_e}}. \quad (3)$$

Here, λ_{ea} is the mean free path of the electrons and $\tilde{T}_e = T_e/T_i$. Possible energy loss caused by diffusion to the tube walls and successive recombination[34], which is hardly possible to estimate accurately, can only decrease τ_{T_e} even more. Hence, Equation 3 provides an upper limit for τ_{T_e}.

The model described above is only valid if the particles can adapt their charge to plasma changes in the spatial afterglow, *i.e.* $\tau_Z < \tau_{pp}$. Since $\tau_{pp} \propto /\sqrt{\tilde{n}}$ and $\tau_Z \propto 1/\tilde{n}$, τ_Z will exceed τ_{pp} for densities below $(\tau_Z^0/\tau_{pp}^0)^2 n_{e,i} = 2 \times 10^{11}\,\mathrm{m}^{-3}$. This density limit is close to the free diffusion regime, where the diffusion of ions and electrons is no longer governed by ambipolar diffusion. This regime starts when the ratio $\lambda_D/\Lambda \sim 1$, where $\Lambda \approx W/\pi$ is the diffusion length. Λ is evaluated assuming cylindrical geometry where W is the width of the glass tube (see Figure 1).

The main parameter that determines the particle charge in our spatial plasma afterglow is T_e. It is likely that $T_e \sim T_i$ at the position of charge measurement. We support this statement with three arguments. Firstly, the model shows that $\tau_{T_e} \ll \tau_I = L/v_{p,f}$, where τ_I is the time that the particles reside in the plasma and L the distance between the active plasma region and the position of particle charge measurement (see Figure 1). Secondly, we showed that the local RF electric strength at the bottom of the setup is small, $E_{RF} \approx 0.1\,\mathrm{V\,m}^{-1}$. Realizing that the electron mean free path $\lambda_{ea} \approx 2\,\mathrm{mm}$, heating of electrons is negligible at this position in the afterglow. Thirdly, there are no resonant electron attachment processes on vacuum impurities close to $\tilde{T}_e \sim 1$[35–37]. In conclusion, the output of our model, according to OML theory, is the particle charge at the late stage of the afterglow $Q_m = -175\,\mathrm{e}$.

Both the measured charge $Q = (-30 \pm 7)\,\mathrm{e}$ and the model-predicted charge $Q_m = -175\,\mathrm{e}$ indicate particle charges that are significantly lower compared to the situation in the plasma bulk which is explained by our model. The fact that they deviate by a factor of six from one another could be due to plasma shielding, the transition from ambipolar to free diffusion, collisionality corrections in the ion flux to the particle surface and the presence of anions. These mechanisms and their relative importance will be discussed subsequently below.

Firstly, in order to exclude the possibility of plasma shielding[2], the measured horizontal acceleration as function of the average horizontal distance of the particles between the electrodes is plotted in Figure 2c. If there would be plasma present between the electrodes, the acceleration must vary with the distance (since the particle charge scales with the plasma potential). However, both the data with (in red) and without (in blue) externally applied electric field show the same slope. Therefore, we can conclude that there is no significant amount of plasma present between the electrodes to effect our measurements. This statement is supported by the particle trajectories and quadratic fits shown in Figure 2b which overlap clearly indicating that the particles do not decharge during the typical 0.1 s measurement time.

Secondly, in the free diffusion regime the ratio $n_i/n_e > 1$ because electrons diffuse faster than ions which causes the particles to decharge with respect to Q_m. Couedel *et al.*[24] have shown that the transition to free diffusion influences the particle charge.

Thirdly, collisionality which could influence the ion current to the particle is not taken into account in the decharging model. For $\lambda_D/\lambda_{ia} \approx 10^{-1}$, the particle charge is lowered because the ion current to the particle surface is increased due to a longer residence time of ions around the particles[2,38]. For increasing λ_D/λ_{ia} the particle charge becomes more negative since the ion current is reduced by ion-neutral collisions. This effect could change Q by a factor 2-3 as compared to the OML particle charge[2,38] and therefore it is likely that collisionality is not the only mechanism accounting for the difference between measurements and model.

Finally, the presence of anions could influence the particle decharging because the current of these anions to the particle surface would directly influences the charging. However, since production of anions can only occur for T_e of several eV[35–37] and since the lifetime of the dominant anions that could be present in our setup is much smaller than τ_I[39], the influence of anions is negligible.

In conclusion, we have measured the charge of microparticles $(-30 \pm 7)\,\mathrm{e}$ in a low pressure spatial plasma afterglow at 0.55 m from the active plasma region which is three orders lower than the particle surface charge expected in bulk plasma. A relatively simple model was developed and applied to this plasma geometry, and was able to qualitatively explain the great difference in particle charge between the bulk and afterglow region.

This research was financially supported by VDL Enabling Technologies Group.

REFERENCES

[1] D. Martin Knotter and F. Wali, *Dev. Surf. Contam. Clean. Part. Depos. Control Remov.*, first edit ed. (Elsevier Inc., 2010) pp. 81–120.

[2] S. Khrapak and G. Morfill, Contrib. to Plasma Phys. **49**, 148 (2009).

[3] J. Beckers, T. Ockenga, M. Wolter, W. W. Stoffels, J. Van Dijk, H. Kersten, and G. M. Kroesen, Phys. Rev. Lett. **106**, 1 (2011).

[4] J. Beckers, D. J. M. Trienekens, and G. M. W. Kroesen, Phys. Rev. E - Stat. Nonlinear, Soft Matter Phys. **88**, 1 (2013).

[5] M. Chaudhuri, S. A. Khrapak, R. Kompaneets, and G. E. Morfill, IEEE Trans. Plasma Sci. **38**, 818 (2010), arXiv:1010.4435.

[6] G. E. Morfill, B. M. Annaratone, P. Bryant, A. V. Ivlev, H. M. Thomas, M. Zuzic, and V. E. Fortov, **44**, 263 (2002).

[7] D. Vollath, J. Nanoparticle Res. **10**, 39 (2008).

[8] A. Bouchoule, *Dusty Plasmas: Physics, Chemistry and Technological Impacts in Plasma Processing* (John Wiley & Sons Inc. New York, 1999) pp. 1–27.

[9] H. Kersten, H. Deutsch, and G. M. Kroesen, Int. J. Mass Spectrom. **233**, 51 (2004).

[10] S. Ratynskaia, S. Khrapak, a. Zobnin, M. H. Thoma, M. Kretschmer, a. Usachev, V. Yaroshenko, R. a. Quinn, G. E. Morfill, O. Petrov, and V. Fortov, Phys. Rev. Lett. **93**, 8 (2004).

[11] C. Zafiu, A. Melzer, and A. Piel, Phys. Rev. E - Stat. Physics, Plasmas, Fluids, Relat. Interdiscip. Top. **63**, 1 (2001).

[12] E. B. Tomme, D. A. Law, B. M. Annaratone, and J. E. Allen, Phys. Rev. Lett. **85**, 2518 (2000).

[13] X. Tang and G. Delzanno, Phys. Plasmas **21**, 123708 (2014), arXiv:arXiv:1503.07820v1.

[14] T. H. Van De Ven, P. Reefman, C. A. De Meijere, R. M. Van Der Horst, M. Van Kampen, V. Y. Banine, and J. Beckers, J. Appl. Phys. **123** (2018), 10.1063/1.5017303.

[15] R. M. Van Der Horst, J. Beckers, E. A. Osorio, and V. Y. Banine, J. Phys. D. Appl. Phys. **48** (2015), 10.1088/0022-3727/48/43/432001.

[16] R. M. Van Der Horst, J. Beckers, E. A. Osorio, D. I. Astakhov, W. J. Goedheer, C. J. Lee, V. V. Ivanov, V. M. Krivtsum, K. N. Koshelev, D. V. Lopaev, F. Bijkerk, and V. Y. Banine, J. Phys. D. Appl. Phys. **49** (2016), 10.1088/0022-3727/49/14/145203.

[17] D. I. Astakhov, W. J. Goedheer, C. J. Lee, V. V. Ivanov, V. M. Krivtsun, K. N. Koshelev, D. V. Lopaev, R. M. van der Horst, J. Beckers, and F. Bijkerk, J. Phys. D. Appl. Phys. **49**, 295204 (2016).

[18] J. P. Allain, M. Nieto, A. Hassanein, V. Titov, P. Plotkin, M. Hendricks, E. Hinson, C. Chrobak, M. H. L. van der Velden, and B. Rice, Spie **6151** (2006), 10.1117/12.656652.

[19] B. Wu and A. Kumar, J. Vac. Sci. Technol. B Microelectron. Nanom. Struct. **25**, 1743 (2007).

[20] A. V. Ivlev, M. Kretschmer, M. Zuzic, G. E. Morfill, H. Rothermel, H. M. Thomas, V. E. Fortov, V. I. Molotkov, A. P. Nefedov, A. M. Lipaev, O. F. Petrov, Y. M. Baturin, A. I. Ivanov, and J. Goree, Phys. Rev. Lett. **90**, 55003 (2003).

[21] L. Couëdel, M. Mikikian, L. Boufendi, and a. Samarian, Phys. Rev. E **74**, 026403 (2006).

[22] L. Couëdel, A. Mezeghrane, B. James, M. Mikikian, A. Samarian, M. Cavarroc, Y. Tessier, and L. Boufendi, 34th EPS Conf. Plasma Phys. 2007, EPS 2007 - Europhys. Conf. Abstr. **31**, 68 (2007).

[23] L. Couëdel, A. A. Samarian, M. Mikikian, and L. Boufendi, EPL (Europhysics Lett. **84**, 35002 (2008).

[24] L. Couëdel, A. A. Samarian, M. Mikikian, and L. Boufendi, Phys. Plasmas **15** (2008), 10.1063/1.2938387.

[25] L. Couëdel, A. Mezeghrane, A. A. Samarian, M. Mikikian, Y. Tessier, M. Cavarroc, and L. Boufendi, Contrib. to Plasma Phys. **49**, 235 (2009).

[26] I. I. Filatova, F. M. Trukhachev, and N. I. Chubrik, Plasma Phys. Reports **37**, 1042 (2011).

[27] B. Layden, L. Couëdel, A. A. Samarian, and L. Boufendi, IEEE Trans. plasma Sci. (2011).

[28] L. P. T. Schepers, W. L. IJzerman, and J. Beckers, J. Phys. D. Appl. Phys. **51**, 375203 (2018).

[29] L. C. J. Heijmans and S. Nijdam, EPL (Europhysics Lett. **114**, 64004 (2016).

[30] V. Lee, S. R. Waitukaitis, M. Z. Miskin, and H. M. Jaeger, Nat. Phys. **11**, 733 (2015).

[31] W. Rogowski, Arch. Electrotech **12** (1923).

[32] S. A. Khrapak, A. P. Nefedov, O. F. Petrov, and O. S. Vaulina, Phys. Rev. E - Stat. Physics, Plasmas, Fluids, Relat. Interdiscip. Top. **59**, 6017 (1999).

[33] Y. P. Raizer, *Gas Discharge Physics* (Springer, Berlin, 1991).

[34] I. Denysenko, I. Stefanović, B. Sikimić, J. Winter, N. A. Azarenkov, and N. Sadeghi, J. Phys. D. Appl. Phys. **44** (2011), 10.1088/0022-3727/44/20/205204.

[35] Y. Itikawa, J. Phys. Chem. Ref. Data **38**, 1 (2009).

[36] D. J. Haxton, C. W. McCurdy, and T. N. Rescigno, Phys. Rev. A - At. Mol. Opt. Phys. **75**, 1 (2007), arXiv:0710.0008.

[37] L. M. Branscomb, Sep. Isol. fractions Rabbit gamma-globulin Contain. Antib. Antigen. Comb. sites **182**, 248 (1958).

[38] S. A. Khrapak, G. E. Morfill, A. G. Khrapak, and L. G. D'Yachkov, Phys. Plasmas **13** (2006), 10.1063/1.2201538.

[39] A. H. Harrison, *Chemical Ionization Mass Spectrometry*, 2nd ed. (CRC press LCC, 1992).